

Article

## Development of a Hydrogen Peroxide Sensor Based on Screen-Printed Electrodes Modified with Inkjet-Printed Prussian Blue Nanoparticles

Stefano Cinti <sup>1</sup>, Fabiana Arduini <sup>1</sup>, Danila Moscone <sup>1</sup>, Giuseppe Palleschi <sup>1</sup> and Anthony J. Killard <sup>2,\*</sup>

<sup>1</sup> Dipartimento di Scienze e Tecnologie Chimiche, Università di Roma Tor Vergata, Via della Ricerca Scientifica 1, Rome 00133, Italy; E-Mails: Stefano.Cinti@uniroma2.it (S.C.); Fabiana.Arduini@uniroma2.it (F.A.); Danila.Moscone@uniroma2.it (D.M.); Giuseppe.Palleschi@uniroma2.it (G.P.)

<sup>2</sup> Department of Biological, Biomedical and Analytical Sciences, Faculty of Health and Applied Sciences, University of the West of England, Coldharbour Lane, Bristol BS16 1QY, UK

\* Author to whom correspondence should be addressed; E-Mail: tony.killard@uwe.ac.uk; Tel.: +44-117-328-2147; Fax: +44-117-344-2904.

Received: 13 June 2014; in revised form: 16 July 2014 / Accepted: 23 July 2014 /

Published: 4 August 2014

---

**Abstract:** A sensor for the simple and sensitive measurement of hydrogen peroxide has been developed which is based on screen printed electrodes (SPEs) modified with Prussian blue nanoparticles (PBNPs) deposited using piezoelectric inkjet printing. PBNP-modified SPEs were characterized using physical and electrochemical techniques to optimize the PBNP layer thickness and electroanalytical conditions for optimum measurement of hydrogen peroxide. Sensor optimization resulted in a limit of detection of  $2 \times 10^{-7}$  M, a linear range from 0 to 4.5 mM and a sensitivity of  $762 \mu\text{A} \cdot \text{mM}^{-1} \cdot \text{cm}^{-2}$  which was achieved using 20 layers of printed PBNPs. Sensors also demonstrated excellent reproducibility (<5% rsd).

**Keywords:** hydrogen peroxide; Prussian blue nanoparticles; screen-printed electrode; inkjet printing

---

## 1. Introduction

The effective measurement of hydrogen peroxide remains a critical analytical goal due to its widespread use in various fields such as food processing, the textile industry, pulp and paper bleaching, pharmaceutical research, clinical chemistry, antiseptic and disinfecting agents [1–3].  $\text{H}_2\text{O}_2$  is also involved in several biological events and intracellular pathways and is the by-product of enzymatic processes such as those involving, for example, glucose oxidase, cholesterol oxidase and alcohol oxidase.  $\text{H}_2\text{O}_2$  is also a substrate for the enzyme horseradish peroxidase [4]. Reliable, accurate, sensitive, rapid, and cost-effective determinations of  $\text{H}_2\text{O}_2$  continue to be widely investigated.

Several analytical techniques including spectrophotometry [5], chemiluminescence [6] and fluorescence [7] have been employed in the determination of  $\text{H}_2\text{O}_2$ . However, most of them exhibit their own technical drawbacks such as being time consuming, complicated or requiring expensive instrumentation. The area of printed electrochemical sensors has proven successful for the detection of many analytes owing to their sensitivity, selectivity, fast response, ease of use and cost-effectiveness. Together with progress in the field of nanomaterials, sensors are an excellent choice in the realization of the accurate and sensitive detection of  $\text{H}_2\text{O}_2$ . Significant effort has been expended on the design of novel  $\text{H}_2\text{O}_2$  sensing techniques and the improvement of their analytical performances.

A wide range of materials such as redox proteins, transition metals and redox polymers have been employed to perform electrocatalytic  $\text{H}_2\text{O}_2$  detection [8–11]. Ferric hexacyanoferrate or Prussian blue (PB) has been referred to as an “artificial peroxidase” [12]. It is electrochemically reduced to form Prussian white (PW), which is capable of catalyzing the reduction of hydrogen peroxide at low potentials (around 0 V vs. Ag/AgCl), which is an excellent characteristic as it allows it to work in the presence of a wide range of interferences. There are several methods in the literature for producing PB. Almost all of the procedures adopted for deposition on electrode surfaces are based on electrochemical techniques [13] or *in situ* chemical deposition [14]. However, PB itself can also be fabricated into different nanostructures. Prussian blue nanoparticles (PBNPs) have received increasing attention in the electrochemical sensor field due to their enhanced surface to volume ratio and increased electrochemical properties associated with their use. The properties of nanoparticles are influenced by the type of synthesis and also by the type of chemical environment which characterizes them. For this reason, different types of PBNPs have been developed that can be produced alone [15] or in the presence of other nanomaterials in order to constitute a hybrid nanocomposite [16,17] each characterized by particular properties.

However, the fabrication of sensors can require several steps and each step introduces variability in the performance of the resulting sensors. This necessitates the development of fabrication procedures which are rapid and simple while also being highly reproducible. The use of printing techniques has been applied to the fabrication of electrochemical sensors for two decades now. In recent times, inkjet printing has become a powerful deposition technology for the fabrication of sensors. This deposition methodology has the capability to deliver precisely patterned quantities of ink at picolitre drop volumes and is now widely used as a tool for device fabrication [18–20]. The deposition of nanomaterial-based inks using inkjet printing has become a key technology for printed electronics [21].

The aim of this work was to develop an electrochemical sensor for the determination of  $\text{H}_2\text{O}_2$  which would be simple and low cost to manufacture while also having excellent analytical performance, by

depositing PBNPs onto screen-printed electrodes using inkjet printing. To the best of our knowledge, Hu *et al.* [22] reported an inkjet printing process to fabricate sensing devices for  $\text{H}_2\text{O}_2$  based on PBNPs. However, this work reports important improvements in terms of sensitivity, detection limit, linear range and reproducibility regarding the determination of  $\text{H}_2\text{O}_2$ .

## 2. Experimental Section

### 2.1. Screen-Printed Electrode Fabrication

Screen-printed electrodes were produced with a 245 DEK (Poole, UK) screen-printing machine [23,24] using graphite-based conductive ink (Electrodag 421) for the working and counter electrode and Ag/AgCl conductive ink (Electrodag 477 SS) for the pseudo-reference electrode, obtained from Acheson (Milan, Italy). The insulating layer was Vinilflat 38.101E from Argon (Milan, Italy). The substrate was a flexible polyester film (Autostat HT5) obtained from Autotype (Milan, Italy). The diameter of the working electrode was 0.3 cm resulting in an apparent geometric area of  $0.07 \text{ cm}^2$ .

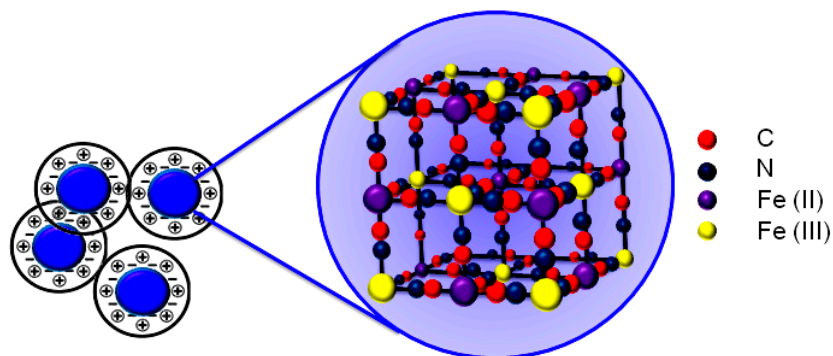
### 2.2. Chemical Reagents

All chemicals from commercial sources were of analytical grade. All solutions were prepared using distilled water.

### 2.3. Preparation of PBNPs Dispersion

The PBNP dispersion was synthesized according to Chen *et al.* [25] by mixing equimolar amounts of potassium ferrocyanide ( $\text{K}_4[\text{Fe}(\text{CN})_6]$ ) and iron (III) chloride ( $\text{FeCl}_3$ ) in presence of HCl in acidic conditions. Briefly, 2 mM  $\text{K}_4[\text{Fe}(\text{CN})_6]$  (2 mL) was mixed with 0.1 M KCl (1 mL) in 10 mM HCl. Subsequently, 2 mM  $\text{FeCl}_3$  (2 mL) was added dropwise into the  $\text{K}_4[\text{Fe}(\text{CN})_6]$  solution under vigorous stirring. A blue solution was gradually formed and the reaction was allowed to proceed overnight to make the reaction complete. The obtained colloid solution was stable for three weeks. A schematic of the structure of the PB crystal is shown in Figure 1.

**Figure 1.** Schematic representation of Prussian blue nanoparticle lattice structure.



#### 2.4. SPE Modification by Inkjet Printing

Inkjet printing was performed using a Dimatix DMP 2831 piezoelectric printer with the Dimatix Drop Manager software (FUJIFILM Dimatix Inc., Santa Clara, CA, USA) a drop spacing of 20  $\mu\text{m}$  using all 16 nozzles. Inkjet-printed sensors were stored dry at room temperature up to 2 months without any loss of activity towards hydrogen peroxide detection.

#### 2.5. Apparatus

Electrochemical measurements were carried out using a Bio-Logic SP-200 potentiostat equipped with EC-Lab<sup>®</sup> software (Bio-Logic Science Instruments, Claix, France). UV-Vis measurements were obtained using a Lambda Bio spectrophotometer (Perkin Elmer, Waltham, MA, USA). Micrographs of the bare SPE and modified SPE with PBNPs were obtained by field emission scanning electron microscopy (FEG-SEM, Leo Supra 35, Oberkochen, Germany).

### 3. Results and Discussion

#### 3.1. Physical and Electrochemical Characterization of Prussian Blue Nanoparticle-Modified Electrodes

The dispersion of PBNPs was characterized using UV-visible spectroscopy and scanning electron microscopy (SEM). The UV-visible spectra of the diluted PBNPs (Figure 2) revealed a broad band centered at 700 nm due to the  $\text{Fe}^{\text{II}}$  to  $\text{Fe}^{\text{III}}$  charge-transfer, characteristic of Prussian blue as seen in previous literature [26]. The synthetic precursor materials showed little distinctive absorption properties across this wavelength range. Screen-printed carbon electrodes (SPEs) were also analysed by SEM before and after deposition of the PBNP ink (Figure 3). Following deposition, the graphitic flakes were covered by a reasonably homogeneous layer of PBNPs with an average diameter of 15 nm and variation of approximately 12%.

**Figure 2.** UV-vis spectra of the PBNP dispersion and its precursors.

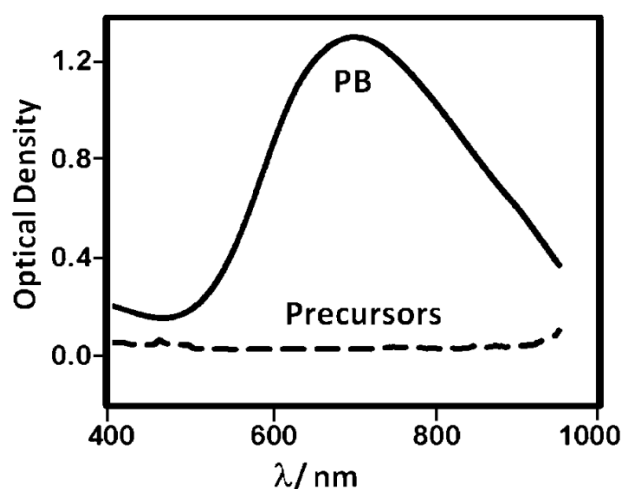
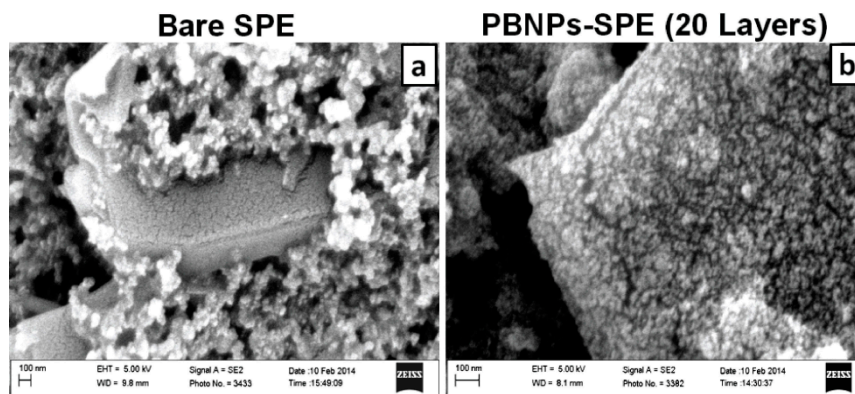


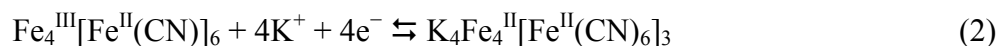
**Figure 3.** Scanning electron micrographs of (a) bare SPE and; (b) SPE modified with 20 inkjet-printed layers of PBNPs. Acceleration voltage: 5 keV, magnification 10 k.



The effect of the quantity of PBNPs deposited onto the SPEs on the electrochemical properties of the sensors was investigated by performing different numbers of prints. Electrodes were modified with 5, 10, 20 and 30 layers of the PBNP solution. Cyclic voltammetric analysis of the sensors was performed in 0.05 M phosphate buffer containing 0.1 M KCl (pH 7.4) at scan rates between 10 and 1000 mV vs. Ag/AgCl in the potential range from  $-0.3$  V to  $0.5$  V (Figure 4). A pair of redox peaks can be seen which are due to the oxidation and reduction of Prussian blue in which the PB is reduced to PW which is re-oxidized to PB. PB is known to exist in both a soluble and insoluble form, according to the following reactions, respectively:



and:



The solubility of PB depends on the ease with which the potassium ion enters and leaves the film. In establishing the properties of the PB film, it is important to establish whether the soluble or insoluble form has been fabricated. There are several methods with which an evaluation of the electron transfer processes involved can be achieved. One method is to employ the peak width at half height ( $\delta_{0.5}$ ), which tends towards  $90.6/n$  mV when both the cathodic and anodic peaks tend to reversibility, where  $n$  is the number of electrons involved [27]. The  $\delta_{0.5}$  was also calculated by taking into account the separation achieved at  $10 \text{ mV}\cdot\text{s}^{-1}$  for the various electrodes, yielding a value of  $21 \pm 0.8$  mV for all four sensors analysed. Peak separation at low scan rate was used to ensure operation in the reversible regime. In this case,  $n$  was found to be equal to  $4.3 \pm 0.3$ , which suggests the presence of the insoluble form of PB (Equation (2)). This reaction involves four electrons and four potassium ions which enter and leave the film in order to ensure charge neutrality of the crystal lattice during the redox process.

Anodic and cathodic peak currents were also related to the number of deposited layers.  $I_{p,a}$  values were 1.11, 7.10, 18.9 and 22.1  $\mu\text{A}$  and  $I_{p,c}$  values were 0.99, 5.901, 17.8 and 18.0  $\mu\text{A}$  for 5, 10, 20 and 30 layers, respectively. Anodic and cathodic currents may vary linearly with scan rate ( $v$ ), or by  $v^{1/2}$ , depending on whether electron transfer processes are surface confined, or whether they depend on diffusion. Figure 5 shows the dependency of the peak current responses of the electrodes on scan rate across the entire scan rate range, and in detail between 0 and  $80 \text{ mV}\cdot\text{s}^{-1}$ , while Figure 6 shows the

dependency of  $I_p$  to  $v^{1/2}$ . This demonstrates that, for fewer layers of PBNPs (5 or 10 prints) at lower scan rates, currents increase linearly with  $v$  and suggest a surface controlled process [28], while for thicker films or at higher scan rates, peak currents were proportional to  $v^{1/2}$  due to the fact that the electrochemical process was controlled by diffusion of the counter ion,  $K^+$ , in the lattice. Table 1 shows the anodic currents and slopes at  $50 \text{ mV}\cdot\text{s}^{-1}$  for different numbers of deposited layers of PBNPs. This data suggests that, while peak current increases with layer thickness, little gain was achieved by moving from 20 to 30 layers, between which, there was also relatively little difference in their electron transfer rates. As a consequence, sensors fabricated with 20 layers were selected for further work.

**Figure 4.** Cyclic voltammograms of PBNP-modified SPEs with (a) 5, (b) 10, (c) 20 and (d) 30 layers. Scan rates were from 10 to  $1000 \text{ mV}\cdot\text{s}^{-1}$  vs. Ag/AgCl in 0.05 M phosphate buffer, 0.1 M KCl, pH 7.4.

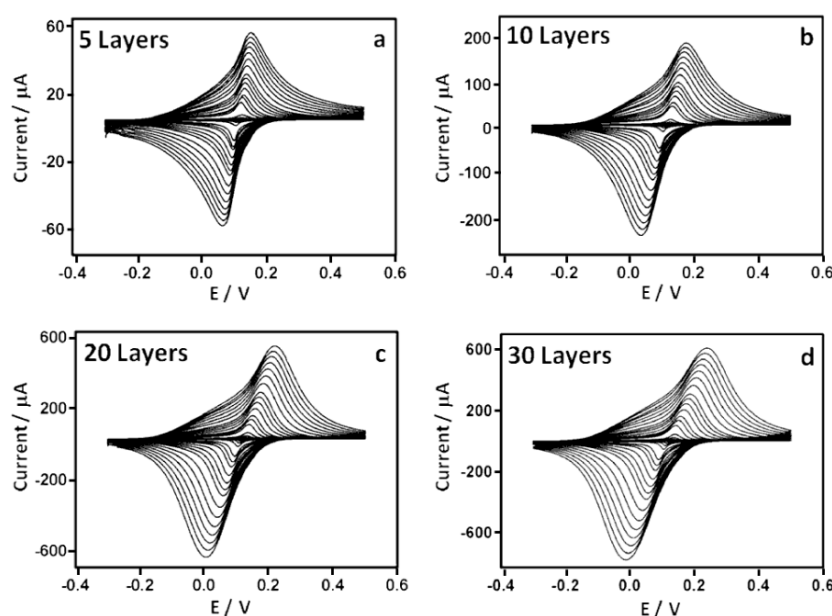


**Figure 5.** (a) Current vs. scan rate ( $10$  to  $1000 \text{ mV}\cdot\text{s}^{-1}$  vs. Ag/AgCl) and; (b) linear correlation between current and scan rate from  $0$  to  $80 \text{ mV}\cdot\text{s}^{-1}$  for PBNPs-SPEs, demonstrating thin layer behavior.

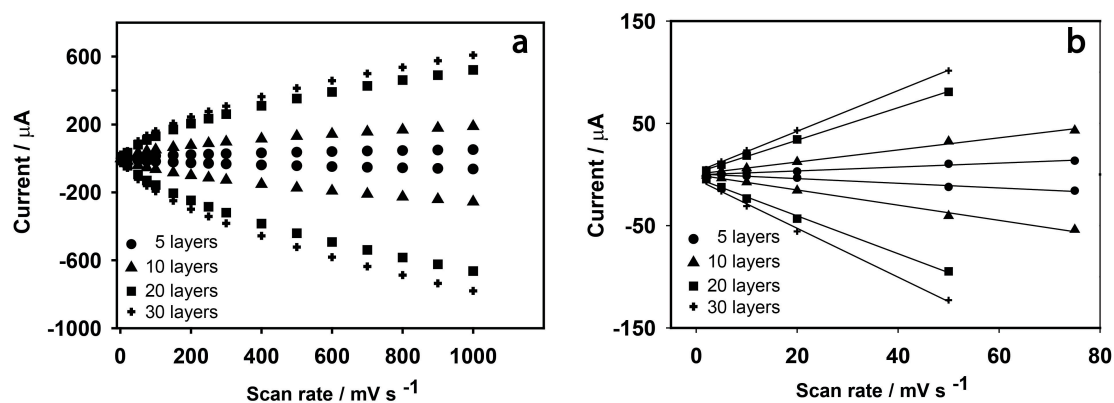


**Figure 6.** Current vs. square root of scan rate for PBNP-SPEs demonstrating the diffusion-controlled behavior.

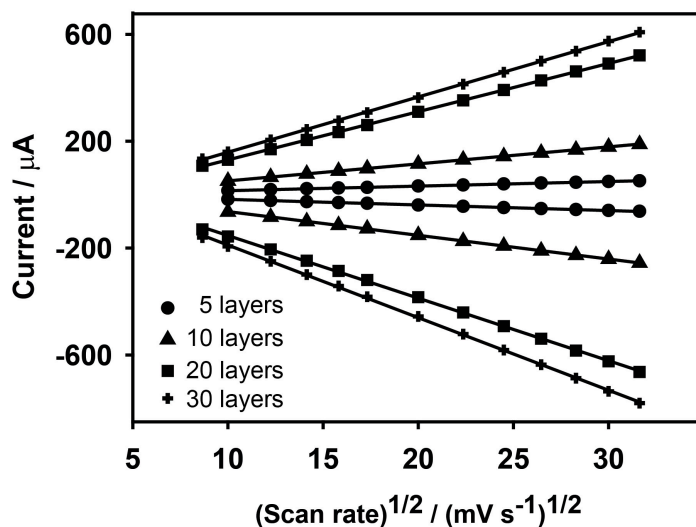


**Table 1.** Summary of electrochemical parameters from scan rate studies ( $50 \text{ mV}\cdot\text{s}^{-1}$  vs. Ag/AgCl) for electrodes modified with different numbers of inkjet-printed layers of PBNPs in 0.05 M phosphate buffer, 0.1 M KCl, pH 7.4.

PBNPs Layers	Anodic Current @ $50 \text{ mV}\cdot\text{s}^{-1}$	Slope (Thin Layer) $\mu\text{A}\cdot\text{mV}^{-1}\cdot\text{s}$	Slope (Diffusion Controlled) $\mu\text{A}\cdot\text{mV}^{-1/2}\cdot\text{s}^{1/2}$
● 5	10.3	0.152	1.69
▲ 10	32.4	0.628	6.37
■ 20	80.8	1.83	17.9
+ 30	101	2.32	20.7

### 3.2. Electrochemical Characterization of Hydrogen Peroxide at a PBNP-SPE

The behavior of PBNP-SPEs toward hydrogen peroxide reduction was investigated using cyclic voltammetry in 0.05 M phosphate buffer containing 0.1 M KCl (pH 7.4) in a potential range from  $-0.1 \text{ V}$  to  $0.3 \text{ V}$  (vs. Ag/AgCl) with a scan rate of  $50 \text{ mV/s}$ . Bare and PBNP-modified SPEs were studied in the presence and absence of  $\text{H}_2\text{O}_2$  (Figure 7). At bare SPEs, there was little or no visible reduction of  $\text{H}_2\text{O}_2$  at the electrode. For PBNP-SPEs, the characteristic redox couple for PB could be seen, while in the presence of  $3 \text{ mM H}_2\text{O}_2$ , the cathodic peak, indicating the formation of PW was shifted to a more negative potential of  $14 \text{ mV}$ , accompanied by an increase in the cathodic current. The anodic peak was also shifted to lower potentials and was reduced in peak current, as expected for mediated, reductive reactions.

These results demonstrate that the PBNP-modified SPEs have electrocatalytic activity towards hydrogen peroxide reduction according to the scheme in Figure 8 and Equations (3) and (4) [12] and related Equations (3) and (4).

**Figure 7.** Cyclic voltammograms of bare SPE in 3 mM H<sub>2</sub>O<sub>2</sub> (solid line), SPE modified with 20 layers of PBNP dispersion in buffer (dashed line) and 3 mM H<sub>2</sub>O<sub>2</sub> (dashed-dotted line). All in 0.05 M phosphate buffer, 0.1 M KCl, pH 7.4 at 50 mV·s<sup>-1</sup> vs. Ag/AgCl.

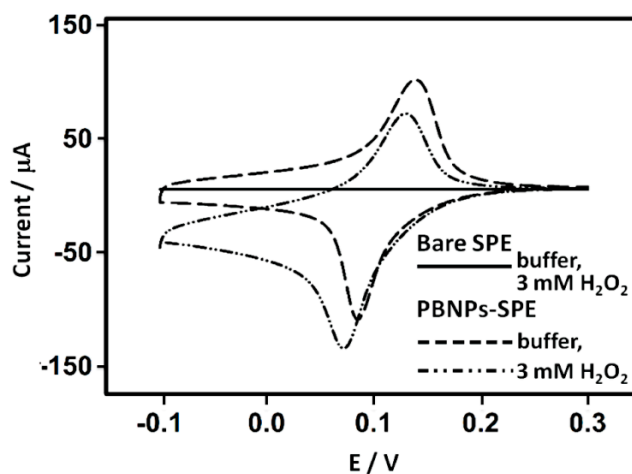
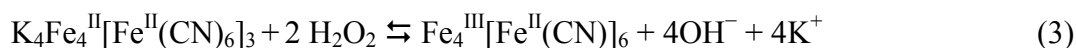
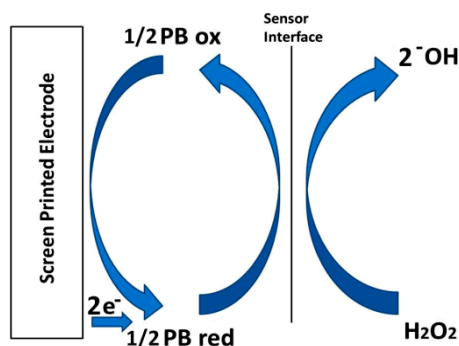


**Figure 8.** Mechanism of the catalytic H<sub>2</sub>O<sub>2</sub> reduction mediated by PB.



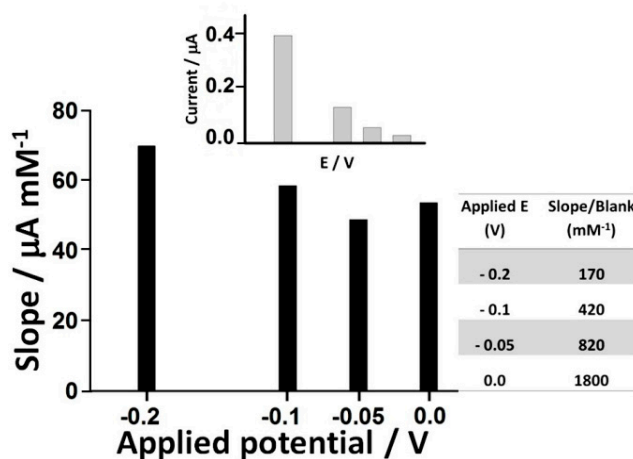
Further work was performed to measure the quantitative response of the sensors to H<sub>2</sub>O<sub>2</sub>.

### 3.3. Amperometric Detection of Hydrogen Peroxide

The choice of the optimum applied potential at the working electrode is essential in achieving the lowest possible limit of detection. Several factors are relevant when making this selection. One is the signal to background ratio of the sensor at a particular potential and the non-faradaic processes that result from a potential step which contributes to the background signal and reduces achievable detection limits. However, this must be balanced against the greater levels of electrolysis that can be achieved at more extreme potentials. The other factor is the likely increase in electrochemical interference at more extreme potentials. The slope to blank ratios of the sensors at 0, -0.05, -0.1 and -0.2 V (vs. Ag/AgCl) are shown in Figure 9. The sensors showed the greatest slope to blank ratio at 0 V, with a response ratio some ten-fold higher than at -0.2 V. This, coupled to the significant

reduction in interference from a number of important reductants at this potential, as reported in a number of earlier studies resulted in a preference for operation of the sensor at 0 V vs. Ag/AgCl [29–31].

**Figure 9.** Selection of the optimum applied potential for the amperometric measurement of H<sub>2</sub>O<sub>2</sub>.



Detailed characterization of the response of the PBNP-SPEs towards H<sub>2</sub>O<sub>2</sub> was performed at 0 V vs. Ag/AgCl pseudoreference on electrodes modified with 20 layers of inkjet-printed PBNPs. Measurements were performed in 0.05 M phosphate buffer containing 0.1 M KCl (pH 7.4) in a stirred batch reaction vessel (n = 6). Limit of detection, linear range, sensitivity and reproducibility were studied (Figure 10). Sensors showed excellent linearity between 0 and 4.5 mM with a detection limit of 0.2 μM, obtained from the formula  $LOD = 3 \cdot \sigma_b / \text{slope}$  ( $r^2 = 0.9994$ ). The sensitivity was 762 μA·mM<sup>-1</sup>·cm<sup>-2</sup>. Furthermore, the sensors showed excellent inter-electrode relative standard deviation of less than 5% for all concentrations tested. As well as the excellent analytical features demonstrated by these electrodes, this is also coupled to the ease and simplicity of their fabrication and amenability to mass production. This compared favorably with several earlier works (Table 2). Hu *et al.* [22] achieved an LOD of 20 μM and a sensitivity of 164.82 μA·M<sup>-1</sup>·cm<sup>-2</sup>. Haghighi *et al.* [15] achieved an analytical range from 2.1 μM to 0.14 mM by using adsorbed PBNPs covered with a layer of Nafion reaching a sensitivity of 138.6 μA·mM<sup>-1</sup>·cm<sup>-2</sup>, but which was more than 5-fold less sensitive than the current sensor, also with a 5-fold higher LOD. Yang *et al.* [32] reported a PB-based electrochemical sensor based on chitosan functionalized with graphene nanosheets, and obtained a similar level of sensitivity to the PBNP inkjet-printed device (816.4 μA·mM<sup>-1</sup>·cm<sup>-2</sup>) but with a higher LOD and narrow linear range (10 μM to 0.4 mM). In other work, Karyakin *et al.* [13] achieved excellent detection limits. However, this was achieved using a gold ultramicroelectrode with electrochemical modification, which requires electrochemical cleaning and deposition processes and so makes mass fabrication challenging. The approach followed by Cao *et al.* [17] also achieved good performance in terms of limit of detection but was also characterized by a long and complex synthesis of the electrocatalyst, while also having a relatively narrow dynamic range. In comparison to other procedures, the inkjet-printed PBNP-modified electrodes certainly represent a good balance between excellent analytical performance and low cost reproducible mass production.

**Figure 10.** Calibration curve of H<sub>2</sub>O<sub>2</sub> on PBNP-SPEs (n = 3) in 0.05 M phosphate buffer, 0.1 M KCl, pH 7.4 at 0 V vs. Ag/AgCl. (a) Detail from 0 to 25 μM and (b) Raw amperometric data from 0 to 4.5 mM.

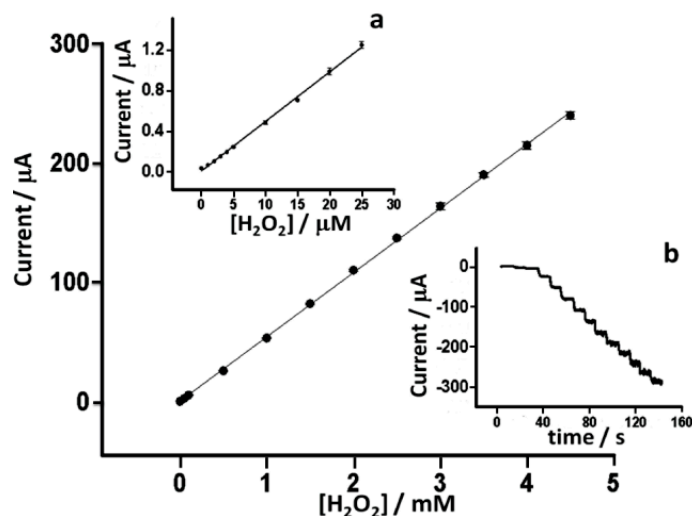


**Table 2.** Analytical performance characteristics of a number of Prussian blue-modified electrodes for H<sub>2</sub>O<sub>2</sub> detection.

Electrode	Modification Procedure	Sensitivity (μA·mM <sup>-1</sup> ·cm <sup>-2</sup> )	LOD (μM)	Linear Range (mM)	Reference
PB-GU E	Electrodeposition	2200	0.01	10 <sup>-5</sup> –1	[13]
Nafion-PBNPs-GE	Dipping	138	1	0.002–0.14	[15]
PBNCs/rGO-GCE	Drop Casting	*	0.045	5 × 10 <sup>-5</sup> –0.12	[17]
PBNPs (100 nm)-SPE	Inkjet	0.164	20	0.02–0.7	[22]
PBNPs (15 nm)-SPE	Inkjet	762	0.2	0.001–4.5	This work

PB-GUμE: Prussian Blue gold ultramicroelectrode (125 μm); GE: Graphite Electrode; PBNCs/rGO-GCE: Prussian Blue NanoCubes on the surface of reduced Graphene Oxide adsorbed on Glassy Carbon Electrode; \* Area of the working electrode has not been reported in the cited paper.

#### 4. Conclusion

The fabrication of sensors for the measurement of H<sub>2</sub>O<sub>2</sub> was achieved using screen-printed electrodes modified with inkjet-printed Prussian blue nanoparticles. Sensors fabricated with 20 inkjet-printed layers were shown to have excellent limits of detection, linear range and reproducibility. The developed sensor represents a simple, robust and reliable means of sensing H<sub>2</sub>O<sub>2</sub> which avoids long and complex multi-step sensor fabrication processes and is suitable for large scale mass production and has many potential applications in environmental, industrial and physiological monitoring, particularly where single use and disposability are advantageous.

#### Acknowledgments

The research leading to these results has received funding from the European Community's Seventh Framework Programme [FP7/2007–2013] under grant agreement no 257372.

## Author Contributions

The laboratory work was carried out by Stefano Cinti under the supervision of Arduini, Moscone and Palleschi in Italy and under Killard in the UK as part of the SIMS FP7 project and contributing towards the PhD thesis of Cinti. The expertise in the fabrication of Prussian blue nanoparticles comes from the laboratory of Palleschi and integrates with expertise in printed sensor technology and cholesterol biosensing with Killard. Cinti was the main contributing author, with significant technical and editorial input from Arduini, Moscone, Palleschi and Killard.

## Conflicts of Interest

The authors declare no conflict of interest.

## References

1. Chen, W.; Cai, S.; Ren, Q.-Q.; Wen, W.; Zhao, Y.-D. Recent advances in electrochemical sensing for hydrogen peroxide: A review. *Analyst* **2012**, *137*, 49–58.
2. Hawe, A.; Wiggenhorn, M.; van de Weert, M.; Garbe, J.H.O.; Mahler, H.-C.; Jiskoot, W. Forced Degradation of Therapeutic Proteins. *J. Pharm. Sci.* **2012**, *101*, 895–913.
3. Niethammer, P.; Grabher, C.; Look, A.T.; Mitchison, T.J. A tissue-scale gradient of hydrogen peroxide mediates rapid wound detection in zebrafish. *Nature* **2009**, *459*, 996–1000.
4. Wang, B.; Zhang, J.-J.; Pan, Z.-Y.; Tao, X.-Q.; Wang, H.-S. A novel hydrogen peroxide sensor based on the direct electron transfer of horseradish peroxidase immobilized on silica–hydroxyapatite hybrid film. *Biosens. Bioelectron.* **2009**, *24*, 1141–1145.
5. Pupo Nogueira, R.F.; Oliveira, M.C.; Paterlini, W.C. Simple and fast spectrophotometric determination of H<sub>2</sub>O<sub>2</sub> in photo-Fenton reactions using metavanadate. *Talanta* **2005**, *66*, 86–91.
6. Hanaoka, S.; Lin, J.-M.; Yamada, M. Chemiluminescent flow sensor for H<sub>2</sub>O<sub>2</sub> based on the decomposition of H<sub>2</sub>O<sub>2</sub> catalyzed by cobalt(II)-ethanolamine complex immobilized on resin. *Anal. Chim. Acta* **2001**, *426*, 57–64.
7. Gomes, A.; Fernandes, E.; Lima, J.L.F.C. Fluorescence probes used for detection of reactive oxygen species. *J. Biochem. Biophys. Methods* **2005**, *65*, 45–80.
8. Wang, Y.; Tang, M.; Lin, X.; Gao, F. Sensor for hydrogen peroxide using a hemoglobin-modified glassy carbon electrode prepared by enhanced loading of silver nanoparticle onto carbon nanospheres via spontaneous polymerization of dopamine. *Microchim. Acta* **2012**, *176*, 405–410.
9. Anjalidevi, C.; Dharuman, V.; Narayanan, J.S. Non enzymatic hydrogen peroxide detection at ruthenium oxide–gold nano particle–Nafion modified electrode. *Sens. Actuators B Chem.* **2013**, *182*, 256–263.
10. Zhang, Z.; Gu, S.; Ding, Y.; Zhang, F.; Jin, J. Determination of hydrogen peroxide and glucose using a novel sensor platform based on Co<sub>0.4</sub>Fe<sub>0.6</sub>LaO<sub>3</sub> nanoparticles. *Microchim. Acta* **2013**, *180*, 1043–1049.
11. Anu Prathap, M.U.; Thakur, B.; Sawant, S.N.; Srivastava, R. Synthesis of mesostructured polyaniline using mixed surfactants, anionic sodium dodecylsulfate and non-ionic polymers and their applications in H<sub>2</sub>O<sub>2</sub> and glucose sensing. *Colloids Surf. B* **2012**, *89*, 108–116.

12. Ricci, F.; Palleschi, G. Sensor and biosensor preparation, optimisation and applications of Prussian Blue modified electrodes. *Biosens. Bioelectron.* **2005**, *21*, 389–407.
13. Karyakin, A.A.; Kuritsyna, E.A.; Karyakina, E.E.; Sukhanov, V.L. Diffusion controlled analytical performances of hydrogen peroxide sensors: Towards the sensor with the largest dynamic range. *Electrochim. Acta* **2009**, *54*, 5048–5052.
14. Arduini, F.; Ricci, F.; Tuta, C.S.; Moscone, D.; Amine, A.; Palleschi, G. Detection of carbamic and organophosphorous pesticides in water samples using a cholinesterase biosensor based on Prussian Blue-modified screen-printed electrode. *Anal. Chim. Acta* **2006**, *580*, 155–162.
15. Haghghi, B.; Hamidi, H.; Gorton, L. Electrochemical behavior and application of Prussian blue nanoparticle modified graphite electrode. *Sens. Actuators B Chem.* **2010**, *147*, 270–276.
16. Li, N.; He, B.; Xu, S.; Yuan, J.; Miao, J.; Niu, L.; Song, J. In site formation and growth of Prussian blue nanoparticles anchored to multiwalled carbon nanotubes with poly(4-vinylpyridine) linker by layer-by-layer assembly. *Mater. Chem. Phys.* **2012**, *133*, 726–734.
17. Cao, L.; Liu, Y.; Zhang, B.; Lu, L. *In situ* controllable growth of Prussian Blue nanocubes on reduced graphene oxide: Facile synthesis and their application as enhanced nano electrocatalyst for H<sub>2</sub>O<sub>2</sub> reduction. *Appl. Mater. Interfaces* **2010**, *2*, 2339–2346.
18. Minemawari, H.; Yamada, T.; Matsui, H.; Tsutsumi, J.; Haas, S.; Chiba, R.; Kumai, R.; Hasegawa, T. Inkjet printing of single-crystal films. *Nature* **2011**, *475*, 364–367.
19. Huang, L.; Huang, Y.; Liang, J.; Wan, X.; Chen, Y. Graphene-based conducting inks for direct inkjet printing of flexible conductive patterns and their applications in electric circuits and chemical sensors. *Nano Res.* **2011**, *4*, 675–684.
20. Hibbard, T.; Crowley, K.; Killard, A.J. Direct measurement of ammonia in simulated human breath using an inkjet-printed polyaniline nanoparticle sensor. *Anal. Chim. Acta* **2013**, *779*, 56–63.
21. Gonzalez-Macia, L.; Morrin, A.; Smyth, M.R.; Killard, A.J. Advanced printing and deposition methodologies for the fabrication of biosensors and biodevices. *Analyst* **2010**, *135*, 845–867.
22. Hu, J.-Y.; Lin, Y.-P.; Liao, Y.-C. Inkjet printed Prussian Blue films for hydrogen peroxide detection. *Anal. Sci.* **2012**, *28*, 135–140.
23. Arduini, F.; Amine, A.; Moscone, D.; Ricci, F.; Palleschi, G. Fast, sensitive and cost-effective detection of nerve agents in the gas phase using a portable instrument and an electrochemical biosensor. *Anal. Bioanal. Chem.* **2007**, *388*, 1049–1057.
24. Cinti, S.; Politi, S.; Moscone, D.; Palleschi, G.; Arduini, F. Stripping analysis of As(III) by means of screen-printed electrodes modified with gold nanoparticles and carbon black nanocomposite. *Electroanalysis* **2014**, *26*, 931–939.
25. Chen, J.; Miao, Y.; Wu, X. Immobilization of Prussian Blue nanoparticles onto thiol SAM modified Au electrodes for analysis of DL-homocysteine. *Colloid J.* **2007**, *69*, 660–665.
26. Uemura, T.; Ohba, M.; Kitagawa, S. Size and surface effects of Prussian blue nanoparticles protected by organic polymers. *Inorg. Chem.* **2004**, *43*, 7339–7345.
27. Laviron, E. General expression of the linear potential sweep voltammogram in the case of diffusionless electrochemical systems. *J. Electroanal. Chem.* **1979**, *101*, 19–28.
28. Bard, A.J.; Faulkner, L.R. *Electrochemical Method Fundamentals and Applications*; Wiley: New York, NY, USA, 1980; Chapter 12, p. 522.

29. Karyakin, A.A.; Karyakina, E.E.; Gorton, L. Amperometric Biosensor for Glutamate Using Prussian Blue-Based “Artificial Peroxidase” as a Transducer for Hydrogen Peroxide. *Anal. Chem.* **2000**, *72*, 1720–1723.
30. Moscone, D.; D’Ottavi, D.; Compagnone, D.; Palleschi, G.; Amine, A. Construction and Analytical Characterization of Prussian Blue-Based Carbon Paste Electrodes and Their Assembly as Oxidase Enzyme Sensors. *Anal. Chem.* **2001**, *73*, 2529–2535.
31. Zou, Y.; Sun, L.-X.; Xu, F. Biosensor based on polyaniline–Prussian Blue/multi-walled carbon nanotubes hybrid composites. *Biosens. Bioelectron.* **2007**, *22*, 2669–2674.
32. Yang, J.-H.; Myoung, N.; Hong, H.-G. Facile and controllable synthesis of Prussian blue on chitosan-functionalized graphene nanosheets for the electrochemical detection of hydrogen peroxide. *Electrochim. Acta* **2012**, *81*, 37–43.

© 2014 by the authors; licensee MDPI, Basel, Switzerland. This article is an open access article distributed under the terms and conditions of the Creative Commons Attribution license (<http://creativecommons.org/licenses/by/3.0/>).